CEAS Aeronautical Journal (2021) 12:605–619
https://doi.org/10.1007/s13272-021-00518-6

ORIGINAL PAPER

Improving a real-time helicopter simulator model with linear input filters

Pavle Šćepanović[1] · **Frederik A. Döring**[1]

Received: 12 February 2021 / Revised: 27 April 2021 / Accepted: 18 May 2021 / Published online: 15 June 2021

Abstract
For a broad range of applications, flight mechanics simulator models have to accurately predict the aircraft dynamics. However, the development and improvement of such models is a difficult and time consuming process. This is especially true for helicopters. In this paper, two rapidly applicable and implementable methods to derive linear input filters that improve the simulator model are presented. The first method is based on model inversion, the second on feedback control. Both methods are evaluated in the time domain, compared to recorded helicopter flight test data, and assessed based on root mean square errors and the Qualification Test Guide bounds. The best results were achieved when using the first method.

Keywords Rotorcraft · System identification · Simulation fidelity · Feedback control

List of symbols

ACT/FHS	Active control technology/flying helicopter simulator
ARS	Air resonance suppression
AVES	Air vehicle simulator
DoF	Degree-of-freedom
FR	Frequency response
MIMO	Multiple-input/multiple-output
PID	Proportional integral derivative
QTG	Qualification test guide
RMS	Root mean square
SISO	Single-input/single-output
$\mathbf{A}, \mathbf{B}, \mathbf{C}, \mathbf{D}$	State, control, output, feedthrough matrices
$\mathbf{x}, \mathbf{u}, \mathbf{y}$	State, control, output vector
δ_x, δ_y	Longitudinal, lateral cyclic pilot controls
δ_p, δ_0	Pedal, collective pilot controls
u, v, w	Translational body velocities
p, q, r	Angular body velocities: roll, pitch and yaw
ϕ, θ, ψ	Roll, pitch and heading angles
a_x, a_y, a_z	Linear accelerations
α, β	Aerodynamic angles of attack and sideslip
ν	Dynamic inflow
a, b	Explicit flapping angles
Ω	Rotor speed
Q	Torque
x_l, y_l, z_l	Regressive lead-lag states
J_{RMS}	Time domain cost function
$n_{\mathrm{o}}, n_{\mathrm{s}}, n_{\mathrm{r}}$	Number of outputs, sample points, and runs
$\mathbf{W}$	Weighting matrix
$\mathbf{u}_{\mathrm{ref}}, \mathbf{y}_{\mathrm{ref}}$	Measured/recorded flight test inputs, outputs
$\Delta(s)$	Input filter (missing dynamics)
$\mathbf{G}(s)$	Transfer function matrix
$\mathbf{G}^{\mathrm{FHS}}(s)$	Linear helicopter model
$\mathbf{G}^{\mathrm{AVES}}(s)$	linear simulator model
$\mathcal{G}^{\mathrm{FHS}}$	Helicopter plant
$\mathcal{G}^{\mathrm{AVES}}$	Simulator plant (baseline)
$\Lambda(s)$	Diagonal low-pass transfer function matrix
a_0	Low-pass filter cutoff frequency
$\tilde{\mathbf{u}}$	Input filter output/shaped simulator commands
$\mathbf{K}(s)$	Linear feedback controller
T_2	Time-to-double
$G^P_{y/u}$	Transfer function model from u to y for plant P

1 Introduction

Helicopter flight simulators are versatile machines that are indispensable in the rotorcraft life cycle. Sophisticated simulators which can successfully recreate aircraft flight and environmental conditions are essential for pilot training, design, and

✉ Pavle Šćepanović
pavle.scepanovic@dlr.de

[1] Institute of Flight Systems, DLR (German Aerospace Center), Lilienthalplatz 7, 38108, Braunschweig, Germany

development of the aircraft, research into its characteristics, control system design, handling qualities, and many more.

The simulation model of the helicopter flight mechanics is the backbone of the flight simulator. Due to its wide field of applications, it is essential that the model correctly represents the actual behavior of the aircraft. Modeling helicopter dynamic response is known to be challenging. Creating a model that realistically predicts a highly coupled, unstable, multi-input multi-output dynamic system such as a helicopter is a difficult task and usually involves many scientists and years of research.

A helicopter flight simulator model typically contains a physics-based nonlinear description of all aircraft components, which effects are then added up in order to solve general differential equations of motion at the center of gravity. In such a model, there is usually a high number of physical parameters that have to be set to appropriate values. A complete set of physical modeling data is often not available and there are many parameters that are difficult to measure exactly. These parameter must be then estimated, which can be a possible source of errors and it can compromise the model fidelity. Furthermore, in order to achieve a satisfactory agreement with flight test data, these parameters are often tuned, which makes the whole process very elaborate and time consuming since it needs to be repeated at various stages of the development process [1].

Improving model fidelity is an active area of research. Ongoing activities include work of NATO Science and Technology Organization AVT-296 Group 'Rotorcraft Flight Simulation Model Fidelity Improvement and Assessment' led by Mark B. Tischler. The group comprises researches from 9 nations and 18 different organizations. The first author of this paper is also a member of the group and this work is a direct contribution to the NATO activities. The objective of the group is to assess the baseline simulation model fidelity and evaluate different methods for model improvement. The AVT-296 working group is a 3-year effort that culminated in a comprehensive report comparing the efficiency of the various assessment and improvement methods based on flight test case studies and provide insight and guidance on their use [2].

This paper is a DLR contribution to Method 2 "Black Box' Input and Output Filter Corrections' of the NATO report. At DLR experience with model fidelity evaluation and model improvements dates back many years ago, but in recent times the technique of inverse simulation evolved as the main tool in augmenting the models obtained through system identification [3, 4]. In [5], inverse simulation is defined as 'a technique whereby the control actions required for a modeled vehicle to fly a specified maneuver can be established'. It is a model-based approach for computing the control inputs needed to obtain the measured output variables. It has been shown that the linear system identified helicopter models could be augmented with an additional linear input filter that reduces the gap between the model outputs and the measured flight test data [4]. Often this input filter is called a 'black-box' correction model, which refers to the non-physical nature of these corrections since they do not represent any known physics but rather the unmodeled 'missing dynamics' or the so-called 'remnants'.

In principle, such correction models can be added at the input side (input filter), in parallel to the baseline model, and at the output side (output filter), see Fig. 1. If the correction model is in parallel or on the output side, care has to be taken to retain physical relationships. For example, if the yaw rate has to be improved, the Euler angles have to be recalculated consistently. In order to avoid this problem, the use of a correction model at the input side is preferred. Input and output filters can be combined in such a way that an input filter is first designed to correct the main deficits of the baseline model and any remaining deficits are then corrected by output filters.

There are two approaches known from the literature to build up the inverse simulation. The first approach calculates an inverse model of the plant either by numerical nonlinear inversion [6] or analytically by linear dynamic inversion [7, 8]. The second one uses a feedback controller and minimizes the response error between simulated and measured output variables [9, 10]. Both approaches can be used for determining the 'residual' control input by calculating the differences between measured controls and the controls obtained from inverse simulation. These differences represent model deficiencies and disturbances and are composed of a deterministic and stochastic part.

This paper presents two methodical and quickly applicable techniques to improve the model fidelity of nonlinear real-time helicopter flight mechanics model based on flight test data. Both techniques use the principles of the aforementioned inverse simulation in obtaining the additional input filter to the simulation model. In this way, the original baseline model isn't directly modified.

In the first approach, the knowledge gained in the last decades in system identification to improve physics-based

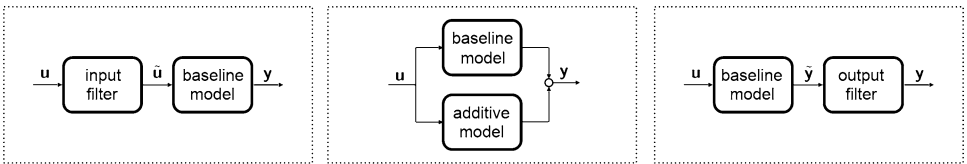

Fig. 1 Possible "black box" update models

simulation models (so-called hybrid modeling) is utilized. In [11], a system identification model of the aircraft was used to calculate the desired input filter for a linear simulator model by algebraic inversion. This paper extends and implements this approach to the nonlinear simulator model.

In the second approach, a model-following controller that approximately inverts the system is used. The controller provides the necessary command response of the desired input filter, which is then fitted with low-order transfer function models in the frequency domain.

The DLR operates the research helicopter Active Control Technology/Flying Helicopter Simulator (ACT/FHS) and the engineering flight simulator Air Vehicle Simulator (AVES) and it will be shown in the next chapter that there is a mismatch between the recorded flight test data and the simulator outputs. A need for a pragmatic method of improving the model fidelity is evident, and reducing this gap is a focal point of this paper. Throughout this study, the research focuses on improving the performance locally i.e. around a given trimmed flight condition in hover and forward flight. Principal concern is model improvement at frequencies below 20 rad/s, since this is the region in which the main dynamics effect are captured with the identified models.

The remainder of this paper is organized as follows: an overview of the helicopter systems and models employed throughout the paper is given in Sect. 2. Two methods for model improvement are described in detail in Sect. 3 and are illustrated on a SISO system example in Sect. 4. The methods will then be applied to the AVES and ACT/FHS data in Sect. 5 and both approaches will be evaluated and discussed in Sect. 6. A final summary and outlook conclude this study in Sect. 7.

2 Helicopter systems and models

This section provides a quick overview of the research helicopter and the engineering simulator at the DLR, the flight test data used in this study, the models of both systems, tools to assess their fidelity, and finally illustrates why there is need for simulator model improvement.

2.1 Active control technology/flying helicopter simulator (ACT/FHS)

The ACT/FHS is a twin-engine, light utility research helicopter with a bearingless main rotor and fan-in-fin tail rotor. Moreover, it is based on Airbus EC135 helicopter but it is a highly modified version and it is not comparable to the standard model. In particular, a full authority fly-by-light control system is used instead of a mechanical control system. More about the ACT/FHS system architecture is given in reference [12].

2.2 Air vehicle simulator (AVES)

The AVES is an engineering flight simulator primarily used as a tool for designing and pre-flight checking of sophisticated control systems and its hardware and software under real-time conditions. Furthermore, it is also used for handling qualities research topics. The experimental hardware and software of the ACT/FHS rotorcraft is replicated in the AVES. More about the AVES system architecture is given in reference [13].

The bare airframe ACT/FHS helicopter is represented in the AVES by a real-time nonlinear flight simulation model. The origin of the model was developed by Hamers and von Grünhagen [14]. It has a classical modular structure dividing the helicopter model into its components, which allows both component-wise validation and simple reconfiguration of single elements. The EC135 configuration data were provided by Eurocopter Deutschland during the ACT/FHS project realization phase. The main rotor is modeled as fully articulated with an equivalent hinge offset and spring restraint in order to represent flapping and lagging natural frequencies. Each main rotor blade is modeled as a rigid blade and blade element theory is used to calculate the aerodynamic forces and moments. Overall, ten blade sections are used to model each blade of the main rotor and the dynamic inflow model of Pitt and Peters is used for the piloted simulation.

2.3 Flight test data

The flight test database used in this paper consists of maneuvers at two speeds (hover and 60 knots). These maneuvers include frequency sweeps (in total 12 for hover, 20 for 60 knots) and 3211 input signals (in total 12 for hover, 16 for 60 knots) in each helicopter control axis and are particularly suited for system identification. The multistep maneuvers include both positive and negative control deflections from the trim point, and amplitudes vary from ± 3 to $\pm 10\%$, and the duration of each run varies between 8 and 12 s. Typically the ACT/FHS helicopter attitude responses in these runs do not have large amplitudes. All system identification flights were flown in the direct mode without the control system assistance in calm air conditions. Raw measured flight test data has been fused and filtered with an unscented Kalman filter [15].

2.4 Linear system models

Linear models of various complexity have been identified both for the ACT/FHS and the AVES. Although it would have been possible to linearize the nonlinear simulation equations numerically, in this paper, a system identification approach was employed to obtain linear AVES models.

These models were created by using a different flight test database than that for the ACT/FHS helicopter. This database consists of automated sweep maneuvers for the identification and computer generated open-loop 3211 maneuvers for the verification. The linear models used in this study describe the ACT/FHS and AVES behavior in hover (0 knots) and forward flight (60 knots) conditions. As usual, state, input, and output variables, $\mathbf{x}, \mathbf{u}$, and $\mathbf{y}$, denote the deviation from trimmed flight condition. All models share the same basic structure

$$\begin{aligned} \dot{\mathbf{x}} &= \mathbf{A}\mathbf{x} + \mathbf{B}\mathbf{u} \\ \mathbf{y} &= \mathbf{C}\mathbf{x} + \mathbf{D}\mathbf{u} \end{aligned} \tag{1}$$

where $\mathbf{A} \in \mathbb{R}^{n\times n}$, $\mathbf{B} \in \mathbb{R}^{n\times 4}$, $\mathbf{C} \in \mathbb{R}^{14\times n}$, and $\mathbf{D} \in \mathbb{R}^{14\times 4}$. The control vector $\mathbf{u} = (\delta_x, \delta_y, \delta_p, \delta_0)^{\mathrm{T}}$ consists of longitudinal and lateral cyclic inputs, δ_x and δ_y, pedal input δ_p, and collective input δ_0. The output vector

$$\mathbf{y} = (u, v, w, p, q, r, \phi, \theta, \dot{p}, \dot{q}, \dot{r}, a_x, a_y, a_z)^{\mathrm{T}} \tag{2}$$

consists of translational body velocities u, v, w, Euler rates p, q, r, Euler angles ϕ, θ, and accelerations $\dot{p}, \dot{q}, \dot{r}, a_x, a_y, a_z$. The state vector $\mathbf{x}$ depends on the model type. For a classical 6-DoF model ($n = 8$), the state vector is completely determined by the rigid body states

$$\mathbf{x}^{\text{6-DoF}} = (u, v, w, p, q, r, \phi, \theta)^{\mathrm{T}}. \tag{3}$$

This classical 6-DoF rigid body model is valid up to about 10 rad/s. In order to arrive at high fidelity models that are valid up to 30 rad/s, the higher-order effects have to be accounted for in order to improve the helicopter cross-coupling prediction capabilities [16]. In addition to the rigid body states, the state vector of the 11-DoF model ($n = 15$) is augmented by $\dot{p}$ and $\dot{q}$ describing the implicit rotor flapping motion, by ν for the dynamic mean inflow, and by four states $x_l, \dot{x}_l, y_l, \dot{y}_l$ which describe the regressive lead-lag blade motion in longitudinal and lateral direction,

$$\mathbf{x}^{\text{11-DoF}} = (u, v, w, p, q, r, \phi, \theta, \dot{p}, \dot{q}, \nu, x_l, \dot{x}_l, y_l, \dot{y}_l)^{\mathrm{T}}. \tag{4}$$

A detailed derivation of the equations of the 11-DoF model can be found in [16, 17]. Finally, the model of 17th order ($n = 17$) augments the 6-DoF state vector with explicit flapping angles a and b, dynamic mean inflow ν, an engine model consisting of rotor speed $\dot{\Omega}_e$, torque Q, and two regressive lead-lag states $z_l, \dot{z}_l$

$$\mathbf{x}^{\text{17ord}} = (u, v, w, p, q, r, \phi, \theta, a, b, \nu, \dot{\Omega}_e, \Omega_e, \Omega, Q, z_l, \dot{z}_l)^{\mathrm{T}}. \tag{5}$$

The engine dynamics improve the yaw rate response to both pedal and collective coupling, especially in hover. A detailed derivation of the equations of the 17th-order model can be found in [18].

All models were identified using the maximum likelihood method in the frequency domain and exhibit an unstable pair of complex poles representing the phugoid motion.

2.5 Model fidelity assessment

In rotorcraft system identification, cost functions proposed in [19, Chap. 12 & 14] are used in time and frequency domain for quantitative model validation. The accuracy of a model in the time domain is typically assessed with the cost function proposed in [19, Chap. 14.3, p. 508]. In order to express model quality, the following variables are used to calculate the root mean square (RMS) error $\mathbf{y}^{\text{RMS}} = [\alpha, \beta, p, q, r, a_x, a_y, a_z, \phi, \theta]$, where α, β are aerodynamic angles of attack and sideslip, respectively. For hover, instead of α and β, reconstructed translational velocities are used. The cost function calculates the difference between simulation results and measurements by computing the square root of the summed, weighted square error for all samples of the output variables, and is defined as

$$J_{\text{RMS}} = \sqrt{\left(\frac{1}{n_{\text{o}} \cdot n_{\text{s}}}\right) \sum_{i=1}^{n_{\text{s}}} [\mathbf{y}_{\text{ref},i}^{\text{RMS}} - \mathbf{y}_i^{\text{RMS}}]^{\mathrm{T}} \mathbf{W} [\mathbf{y}_{\text{ref},i}^{\text{RMS}} - \mathbf{y}_i^{\text{RMS}}]}, \tag{6}$$

where $n_{\text{o}} = 10$ is the number of outputs, n_{s} is the number of time-history sample points in the model data, $\mathbf{W}$ denotes the weighting matrix, and $\mathbf{y}_{\text{ref}}^{\text{RMS}}$ and $\mathbf{y}^{\text{RMS}}$ are the perturbation time-history vectors of the measured (flight test) and simulated data, respectively. The output errors are weighted with $\mathbf{W}$ such that the linear motion variables are given in ft, ft/s, and the rotational ones in °, °s. In [19], guidelines are set for helicopter model accuracy: fidelity can be considered adequate when J_{RMS} is between 1 and 2, and for values smaller than 1 can be considered as good. The overall RMS is calculated as the mean value of J_{RMS} for all runs per flight condition (hover and forward flight), i.e. $(\sum_i^{n_{\text{r}}} J_{\text{RMS}})/n_{\text{r}}$, where n_{r} is the number of runs.

The RMS error is an established, widely accepted, and easy to use performance measure. However, it should not be taken as a definitive statement about the predictive ability of the model. For example, a simple constant offset of 1 m/s in velocity, even with perfect trend tracking, would lead to $J_{\text{RMS}} = 3.28$ (well above acceptable model quality), which corresponds to the conversion of m/s to ft/s.

Simulator manufacturers often refer to Qualification Test Guide (QTG) performance standards. The certification authorities define the acceptable tolerances for simulator model fidelity in the form of QTGs [20]. A flight test data package needed to satisfy the QTG must contain more than one hundred individual events to meet the highest Level-D requirements. QTG maneuvers can be separated into 3 test categories: snapshot test, dynamics test and trajectories

test. Many of these maneuvers are very short (only couple of seconds) and in some control system (typically stability augmentation system) is allowed to be on.

In this paper, the quantitative assessment of the model fidelity is accompanied by using a simplified variant of the least demanding dynamic test category of the QTG. Flight dynamics tests involve a pre-defined control input perturbation at trim condition. In particular, the prescribed tolerances for 3211 multistep inputs are shown in this paper. The reason standard QTG maneuvers aren't used is the unavailability of such flight test data. Thus the QTGs are used solely as a indicator of the usually required model fidelity rating by the certification authorities.

The tolerances (shown in graphs as a shaded area around the flight test data) are defined for longitudinal cyclic input cases as ±10% or 2°s (whichever is easier to achieve) on the pitch rate response and ±1.5° on the pitch attitude change following a control input. For lateral cyclic input cases, a tolerance of ±10% or 3°s on the roll rate response and of ±3° on the roll attitude change following a control input are defined. Similarly, for pedal input, tolerance of ±10% or 3°s on the yaw rate and for collective input a tolerance of ±10% on the vertical velocity following a control input is assigned. It should be noted that for all cases, the off-axis response must show the correct trend.

2.6 Differences between the two systems

Figure 2 compares measured flight test data (ACT/FHS) and simulator model (baseline) response to a lateral 3211 input at 60 knots. The baseline model correctly predicts the trends and the on-axis responses. The response in the lateral velocity is significantly damped in comparison to the measured data. QTG limits are satisfied for the first 5 s, then the model tends to deviate. Off-axis couplings should be improved, especially the yaw rate response.

Figure 3 depicts the measured flight test data (ACT/FHS) and the simulator model (baseline) response to pedal 3211 input, in hover. Here again, the trend of the on-axis response is correct, though the amplitude of the response is much higher than that of the flight data. The roll attitude exhibits a stronger gradient towards the end of the run. In general, the largest differences are observed at the end of almost each run and this probably indicates that the simulation tends to drift away, indicating the instability of the model. QTG limits are not satisfied in hover and are even hardly observable, due to the drift of the model.

Figure 4 shows RMS errors from Eq. (6) for 3211 maneuvers, for each control axis. It demonstrates that the model fidelity does not satisfy the guidelines for adequate fidelity proposed in [19]. This guideline is originally defined for linear models derived by system identification and might be not appropriate in this case. It can be observed that the simulator

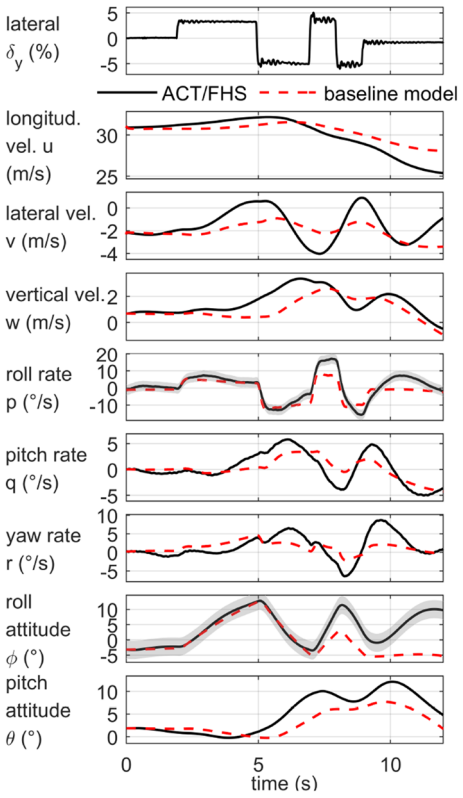

Fig. 2 Time domain comparison between measured flight test data (ACT/FHS) and simulator model (baseline), at 60 knots, lateral 3211 input

performs much better at 60 knots than in hover. Especially the case of lateral input is well predicted for both velocities. Response to longitudinal input is for both velocities characterized by model deficiencies. The overall model fidelity for 60 knots is $J_{\mathrm{RMS}} = 4.78$ and for hover $J_{\mathrm{RMS}} = 7.62$.

3 Methods for determining suitable input filters

In order to compensate for the model deficiencies outlined above, the design of an input filter is proposed shaping commanded inputs to the simulator in such a way that its response better resembles that of the actual helicopter. Figure 5 visualizes this concept. Recorded flight test data $\mathbf{u}_{\mathrm{ref}}$ and $\mathbf{y}_{\mathrm{ref}}$ serve as a reference. The error $\mathbf{e} = \mathbf{y}_{\mathrm{ref}} - \mathbf{y}$ between the recorded outputs $\mathbf{y}_{\mathrm{ref}}$ and the simulator outputs $\mathbf{y}$ should be made as small as possible. To that end, for each flight condition (in this study at hover and at 60 knots forward flight), a suitable 4×4 transfer function matrix $\Delta(s)$ is derived, referred to as input filter or 'missing dynamics'.

In the following two subsections, two approaches are described which accomplish this by using previous knowledge on system models and feedback controller structure.

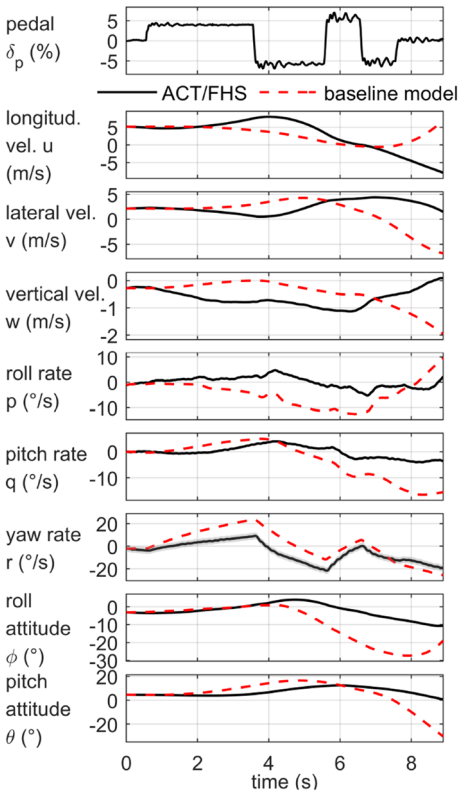

Fig. 3 Time domain comparison between measured flight test data (ACT/FHS) and simulator model (baseline), in hover, pedal 3211 input

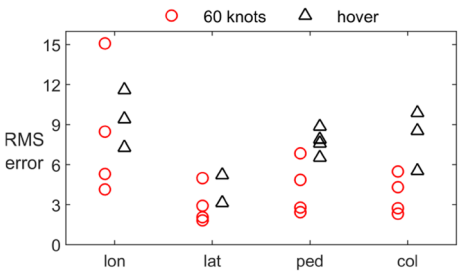

Fig. 4 RMS error for baseline model. The overall error is 4.78 at 60 knots and 7.62 in hover

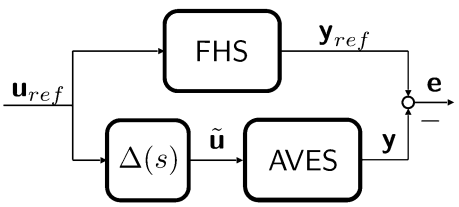

Fig. 5 Conceptual setup for input filter performance evaluation

3.1 Algebraic computation

The first approach uses the linear models of the helicopter and the simulator introduced in Sect. 2.4 and solves for the desired input filter algebraically based on the relations depicted in Fig. 5. For this purpose, four common outputs in both models (denoted by $\hat{\mathbf{C}}$ and $\hat{\mathbf{D}}$) reflecting on-axis responses are selected, such that the system (1) becomes square. Then for each model the transfer function matrix

$$\mathbf{G}(s) = \hat{\mathbf{C}}(sI - \mathbf{A})^{-1}\mathbf{B} + \hat{\mathbf{D}} \tag{7}$$

is calculated where s denotes the Laplace variable. Requiring the error $\mathbf{e} = \mathbf{y}_{\text{ref}} - \mathbf{y}$ between the selected outputs to vanish yields $\mathbf{G}^{\text{FHS}}(s) = \mathbf{G}^{\text{AVES}}(s)\Delta(s)$ or equivalently,

$$\Delta(s) = (\mathbf{G}^{\text{AVES}}(s))^{-1}\mathbf{G}^{\text{FHS}}(s). \tag{8}$$

The resulting $\Delta(s)$ is a 4×4 matrix whose elements are real-rational functions in s. From an algebraic point of view, such a computation is possible if $\mathbf{G}^{\text{AVES}}(s)$ has full rank at all values s except at a finite set of singularities. This is the case since the inputs and outputs of the respective models are independent. However, from a systems theoretic perspective, two aspects need further discussion.

The first one is stability. The number of unstable poles introduced to the system by the input filter $\Delta(s)$ should be as low as possible because it affects how easily the compensated system can be controlled by a pilot. However, unstable poles are not completely avoidable since they are already contained in $\mathbf{G}^{\text{FHS}}(s)$ (phugoid motion). Whether the inverse of $\mathbf{G}^{\text{AVES}}(s)$ is stable or not is determined by its transmission zeros. For minimal realizations as in (1), the transmission zeros are exactly those complex numbers where the corresponding Rosenbrock matrix loses rank [21, Ch. 2.4]. Roughly speaking, finite transmission zeros of a system become finite poles of its inverse [22]. Which and how many transmission zeros occur depends on the choice of the outputs. For the model variants presented in Sect. 2.4 only the common output vector $\mathbf{y} = (\theta, \phi, r, w)^{\text{T}}$ allowed for stable transmission zeros (in which case $\hat{\mathbf{D}} = 0$). The only exception to this is the 11-DoF hover model, where a right half-plane transmission zero at $s = 0.0007$ rad/s is present.

Remark (Time to double amplitude). To estimate how severely an unstable pole might affect the helicopter handling, the time to double amplitude of the unstable (oscillatory) motion can be considered. Let $\lambda \in \mathbb{C}$ denote the unstable pole, then the time to double amplitude is given by $T_2 = \ln(2)/\text{Re}(\lambda)$. As an example, experienced helicopter pilots can handle unstable phygoid modes at hover with a time to double amplitude of just $2 - 4$ s [23]. For the pole mentioned above, $T_2 = \ln(2) \cdot 2 \cdot \pi/(0.0007\ 1/\text{s}) = 8976$ s and is therefore not problematic.

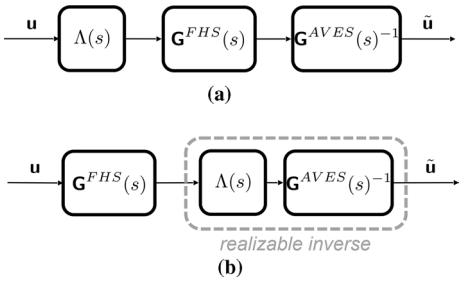

Fig. 6 Different ways of implementing the input filter $\Delta(s)$

The second aspect is the properness of the resulting input filter. It means that for each of the filter's elements, the degree of the numerator polynomial is not larger than the degree of the denominator polynomial. Properness is required for a feasible implementation and can be achieved by multiplying the right-hand-side of (8) with a diagonal 4×4 filter $\Lambda(s)$, see Fig. 6a). Its diagonal elements are low-pass filters

$$\Lambda(s)_{jj} = (a_0/(s + a_0))^{k_j}, \quad j \in \{1, 2, 3, 4\} \tag{9}$$

of appropriate order k_j. Using additional low-pass filters is a common approach to deal with improper systems, for example, when implementing PID controllers [24, Ch. 10.1]. Experiments showed that $a_0 = 20$ rad/s yields a good compromise between accuracy and control effort. If one wishes to study the effect of the inverse AVES model separately, one has to implement the structure depicted in Fig. 6b). This, however, is beyond the scope of the paper. A minimal state-space realization of $\Delta(s)$ is most convenient for implementation purposes.

3.2 Estimation via controller response

The second approach resorts to feedback control, which yields input signals that are subsequently used to identify a suitable input filter.

Figure 7 shows the setup, a standard 2-DoF control configuration. The helicopter and the simulator plant are denoted by $\mathcal{G}^{\text{FHS}}$ and $\mathcal{G}^{\text{AVES}}$, respectively. Recorded flight test data is replayed and fed into the loop as reference $\mathbf{y}_{\text{ref}}$ and as feedforward signal $\mathbf{u}_{\text{ref}}$. All measurements are processed through a sensor data fusion based on an unscented Kalman filter. The feedback controller is designed as a model-following controller and provides the necessary (off-axis) responses. It exhibits cascaded PID-like structures for all four axes without cross-axis couplings. These components were developed and tested as part of a comprehensive pilot assistance system [25].

As an example, Fig. 8 depicts the controller structure for the lateral axis. It consists of an inner loop controlling the roll angle ϕ (with additional feedback of roll rate p and its derivative) and an outer loop controlling lateral velocity v_{r}. An air resonance suppression (ARS) filter prevents the excitation of the regressive lead-lag dynamics. It basically inverts the lead-lag dynamics of the helicopter and is only present in the lateral control axis [26]. The longitudinal axis structure is identical: the pitch angle θ (with additional feedback of pitch rate q and its derivative) is controlled in the inner loop while the outer loop controls the forward velocity. The yaw axis has only one (inner) loop for controlling the yaw rate r and the heading ψ. Finally, the heave axis controls the downward velocity in the geodetic helicopter frame with a PI controller.

The desired closed-loop performance is determined by the agility of the plant to be followed. For example, at 60 knots forward flight, a pitch bandwidth of 3 rad/s, a roll bandwidth of 4 rad/s, a yaw bandwidth of 3 rad/s and a heave response characterized by a first-order transfer

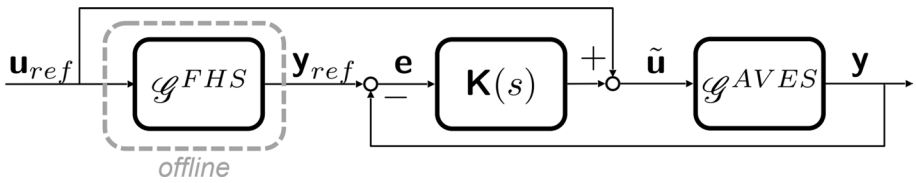

Fig. 7 Feedback controller structure

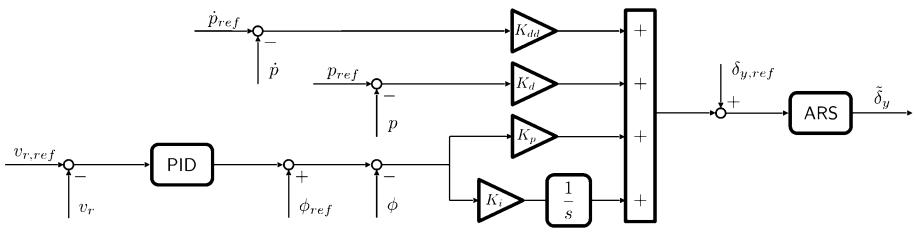

Fig. 8 Controller for the lateral axis

function with a time constant of 0.5 s and a delay of 0.1 s is sufficiently fast to follow the open-loop ACT/FHS response [27].

Remark Consider Fig. 7 and assume that the simulator $\mathcal{G}^{\text{AVES}}$ behaves approximately linear around a given trim point, then the controller response can be calculated as

$$\tilde{\mathbf{u}} = \mathbf{K}(\mathbf{y}_{\text{ref}} - \mathbf{y}) + \mathbf{u}_{\text{ref}} \tag{10}$$

which together with

$$\mathbf{y} = (\mathbf{I} + \mathcal{G}^{\text{AVES}}\mathbf{K})^{-1}\mathcal{G}^{\text{AVES}}(\mathbf{K}\mathbf{y}_{\text{ref}} + \mathbf{u}_{\text{ref}}) \tag{11}$$

leads to

$$\begin{aligned}\tilde{\mathbf{u}} &= \mathbf{K}y_{\text{ref}} - \mathbf{K}(\mathbf{I} + \mathcal{G}^{\text{AVES}}\mathbf{K})^{-1}\mathcal{G}^{\text{AVES}}(\mathbf{K}y_{\text{ref}} + u_{\text{ref}}) + u_{\text{ref}} \\ &= (\mathbf{I} + \mathbf{K}\mathcal{G}^{\text{AVES}})^{-1}(\mathbf{I} + \mathbf{K}\mathcal{G}^{\text{FHS}})\mathbf{u}_{\text{ref}}.\end{aligned} \tag{12}$$

This means a high-gain controller approximately recovers the expression in (8), here, however, for real plant dynamics.

If reasonable reference trajectories are provided, due to its nature, a feedback controller yields appropriate command inputs that allow a close match between measured references and simulator outputs. In order to enable an equivalent open-loop input filter implementation, a system identification of the controller response is performed. For this purpose, recorded sweep signals were used to provide sufficient excitation over the entire frequency range. For each of the four axes, two sweep signals were fed into the controller structure as a reference, as shown in Fig. 7.

This data was then combined to generate the 4×4 frequency response of the signal path from $\mathbf{u}_{\text{ref}}$ to $\tilde{\mathbf{u}}$. This leads to 16 transfer functions that are identified separately with low-order, stable SISO transfer functions, which are finally concatenated to obtain the desired input filter $\Delta(s)$. The goal is to model the frequency response accurately in a range from 0.1 rad/s up to about 20 rad/s, especially at frequencies where the response magnitude is above −20 dB [4]. A minimal state-space realization is again recommended for the implementation of $\Delta(s)$. However, for this approach, the resulting system order is much higher since the identified SISO transfer functions do usually not share a common denominator.

On the one hand, modeling errors in the identification step will reduce the estimated input filter's overall performance. On the other hand, this identification offers the opportunity to emphasize certain aspects of the data that might be beneficial for designing an input filter but were not captured during the 'regular' system identification of the models in (1). In contrast to Sect. 3.1, this filter design also takes other quantities such as u, v and ψ implicitly into account, since the feedback controller does.

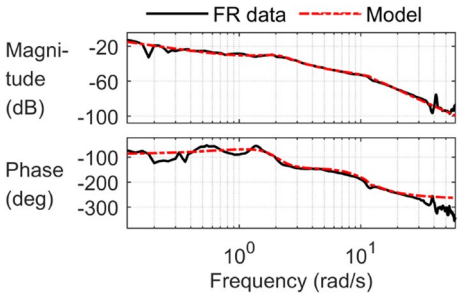

Fig. 9 Lateral frequency response from δ_y to ϕ of the ACT/FHS and identified transfer function $G^{\text{FHS}}_{\phi/\delta_y}$

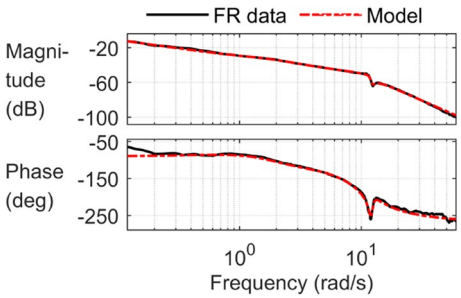

Fig. 10 Lateral frequency response δ_y to ϕ of the AVES and identified transfer function $G^{\text{AVES}}_{\phi/\delta_y}$

4 A single-input single-output example

A simple example shall illustrate the above concepts. The aim here is to improve the lateral response behavior from δ_y to ϕ and p at 60 knots by introducing a SISO input filter.

First, models of the lateral response for both the simulator and the flight test data are identified. Figures 9 and 10 depict the frequency responses and the corresponding identified transfer function models. The models read as

$$G^{\text{FHS}}_{\phi/\delta_y}(s) = \frac{1}{s} \cdot \frac{2.272}{s^2 + 10.61s + 130} \cdot \frac{(s + 2.274)^2}{s^2 + 1.335s + 4.306} \cdot \frac{s^2 + 1.433s + 141.6}{s^2 + 1.284s + 139.2} \tag{13}$$

$$G^{\text{AVES}}_{\phi/\delta_y}(s) = \frac{1}{s} \cdot \frac{2.712}{s^2 + 10.74s + 108.8} \cdot \frac{s^2 + 3.888s + 3.782}{s^2 + 2.737s + 3.617} \cdot \frac{s^2 + 0.944s + 151.6}{s^2 + 1.544s + 139.1} \tag{14}$$

and describe the basic roll response (second factor), the dutch-roll behavior (third factor), and the lead-lag dynamics (fourth factor). The integrator $\frac{1}{s}$ in both equations models the transition from roll rate p to roll attitude ϕ. Applying the

algebraic approach according to Eq. (8), one can calculate the input filter (referred to as 'algebraic $\Delta(s)$') as

$$\Delta_{\tilde{\delta}_y/\delta_y}(s) = (G^{\mathrm{AVES}}_{\phi/\delta_y}(s))^{-1} G^{\mathrm{FHS}}_{\phi/\delta_y}(s) \tag{15}$$

which can be thought of compensation and replacement of the basic roll (hardly recognizable magnitude slope at around 11 rad/s), the dutch-roll (peak at around 2 rad/s), and the lead-lag (sharp peak at around 12.5 rad/s) responses, respectively. Figure 11 shows its Bode diagram. Since both transfer functions have the same number of poles and zeros, an additional low-pass filter is not required.

Applying the second approach, firstly, a feedback controller is designed to achieve proper tracking of the reference signals p_{ref} and ϕ_{ref}. The transfer function in Eq. (14) serves as a design model and since all its zeros are located in the left half-plane, a high-gain design is feasible. It is realized with a PID structure, which, according to Fig. 8, feeds back the roll rate error with gain K_d and controls the roll attitude with PI gains K_p and K_i (K_{dd} is set to zero). The parameters are tuned to yield a good command response; for this example, $K_d = 400$, $K_p = 400$ and $K_i = 40$ is a decent choice. The recorded lateral control signal $\delta_{y,\mathrm{ref}}$ is available as a feedforward command and improves the response quickness. For the sake of completeness, also an air resonance filter was included inverting the lead-lag dynamics in (14).

In this example, for the ease of computation, the AVES is substituted with its linear 11-DoF model at 60 knots. This means that, in the scope of this example, the input filters, as well as the PID controller, are applied to the 11-DoF model rather than to the AVES.

In order to derive an alternative input filter based on the aforementioned PID controller, lateral flight test sweep data was used to excite the controlled system. The resulting controller response from $\delta_{y,\mathrm{ref}}$ to the output $\tilde{\delta}_y$ is then identified with a transfer function model (referred to as 'ctr-based $\Delta(s)$') given by

$$\Delta_{\tilde{\delta}_y/\delta_y}(s) = 0.74 \cdot \frac{s^2 + 2.6s + 6.1}{s^2 + 1.4s + 5.1} \cdot \frac{s^2 + 19.4s + 160.9}{s^2 + 13.7s + 147}. \tag{16}$$

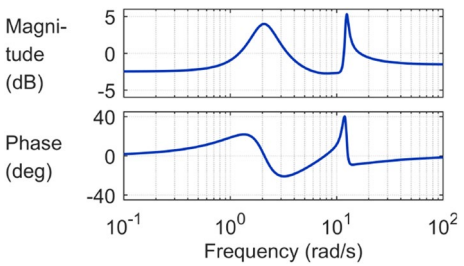

Fig. 11 Bode diagram of input filter $\Delta_{\tilde{\delta}_y/\delta_y}$ ('algebraic $\Delta(s)$')

and depicted in Fig. 12. A comparison with Fig. 11 reveals that both derived input filters roughly capture the same dynamics.

Finally, the expressions in (15) and (16) are implemented as input filters to the 11-DoF model $\mathbf{G}^{\mathrm{AVES}}(s)$ at 60 knots. During the simulation, all inputs were kept to zero except for the lateral input, which is fed by the recorded 3211 flight test data. Figure 13 shows the roll response of the 11-DoF simulator model caused by the filtered lateral control input signals. The roll response is improved by the input filters, which is especially apparent for the roll rate.

Two conclusions can be drawn from this example. Firstly, in simple cases, as studied in this section, it is possible to infer a physical interpretation of the missing dynamics, which are, therefore, by no means a "black box". Secondly, this example demonstrates that, even if all couplings are neglected and only the lateral on-axis response is considered, measurable improvement can still be achieved. This motivates the application of these techniques to multiple-input multiple-output systems, which is discussed in the next section.

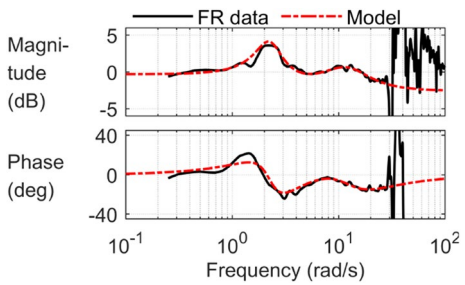

Fig. 12 Bode diagram of controller frequency response from $\delta_{y,\mathrm{ref}}$ to $\tilde{\delta}_y$ and identified input filter $\Delta_{\tilde{\delta}_y/\delta_y}$ ('ctr-based $\Delta(s)$')

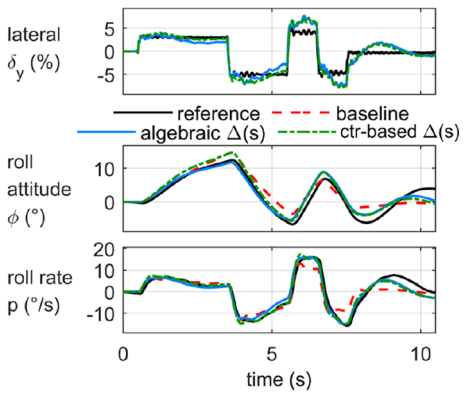

Fig. 13 Roll rate and attitude response due to recorded and filtered lateral control inputs

5 Application to AVES and ACT/FHS

All of the results presented in this chapter have been obtained using the experimental system of the simulator, which itself is a replica of the one in the ACT/FHS [12].

It is important to note that signals fed into the simulator first have to pass the actuators before entering the nonlinear simulation model. However, the recorded flight test inputs come directly from the helicopter's actuators. Ensuring that the simulator data are comparable and consistent with the flight test data, the recorded input data must be preprocessed first. This means that actuator dynamics have to be compensated so that model discrepancies cannot be assigned to the errors in the simulation of the actuators. This is performed using inverse simulation of simulator actuator dynamics, which shifts the data in time axis to the left so that the delay created by the simulator actuator is compensated. More about this study is given in [28].

5.1 Application of algebraic inversion

The efficiency of the approach presented in Sect. 3.1 depends on three points:

- the fidelity of the identified linear helicopter model $\mathbf{G}^{\mathrm{FHS}}(s)$ imposed on the simulator,
- the efficiency of the inverse model $(\mathbf{G}^{\mathrm{AVES}}(s))^{-1}$ to cancel the simulator dynamics,
- the effectiveness of the input filter $\Delta(s)$ to augment the baseline model.

Regarding the first point, the Eq. (6) from Sect. 2.5 to calculate the error between model outputs and flight test data is used. Table 1 shows the overall RMS error values for all model types at both velocities. It can be observed that all models satisfy the guidelines for adequate model fidelity in Sect. 2.5. However, judging model fidelity solely based on the time domain RMS error results can be misleading. Often the 6-DoF model is satisfying for simulation of 3211 runs, but not for the use in control system design. For our work, it is sufficient to know that all models exhibit a good match in time domain simulation and that they are significantly better than the baseline model.

Answering the second point is more challenging. It is clear that the fidelity of the model itself has to be high for the inverse model to be good, but equally important is the effectiveness of the inversion. In order to study this problem, the implementation shown in Fig. 6b) is considered. Here, the identified helicopter model $\mathbf{G}^{\mathrm{FHS}}(s)$ can be simulated separately. Ideally, the inverse model cancels the simulator dynamics and passes the helicopter model outputs to the simulator outputs, without changing them.

Figure 14 shows an exemplary comparison between the flight test data, the linear 6-DoF model $\mathbf{G}^{\mathrm{FHS}}(s)$, and the updated model $\mathcal{G}^{\mathrm{AVES}}\Delta(s)$, at 60 knots to longitudinal input. The comparison is made for only four outputs for which the linear simulator model was inverted. If the inversion works perfectly, the updated model $\mathcal{G}^{\mathrm{AVES}}\Delta(s)$ should produce exactly the $\mathbf{G}^{\mathrm{FHS}}(s)$ outputs. This is, however, not the case and small differences are observed in each output. Table 2 lists the RMS error between the $\mathbf{G}^{\mathrm{FHS}}(s)$ outputs and the updated model outputs (again only for the four inverted outputs). Perfect inversion would mean $J_{\mathrm{RMS}} = 0$. In general, the inversion was effective in passing on-axis responses and for off-axis, discrepancies are observed. Best results were obtained with 6-DoF inverse simulator models $\mathbf{G}^{\mathrm{AVES}}(s)^{-1}$, especially at 60 knots.

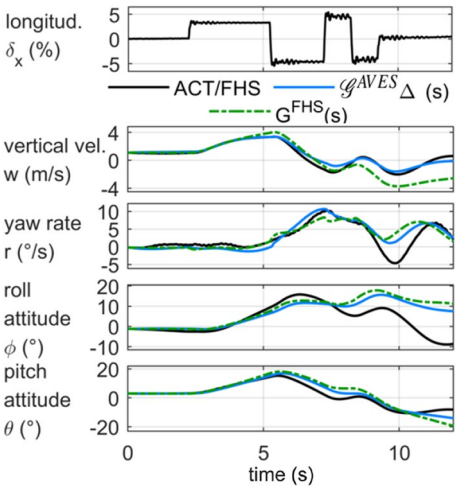

Fig. 14 Effectiveness of the inversion: comparison of the updated simulator model $\mathcal{G}^{\mathrm{AVES}}\Delta(s)$ and identified helicopter model $\mathbf{G}^{\mathrm{FHS}}(s)$ for 6-DoF models at 60 knots

Table 1 Overall RMS error for identified helicopter models $\mathbf{G}^{\mathrm{FHS}}(s)$

	6-DoF	11-DoF	17ord
Hover	1.61	1.61	1.52
60 knots	1.85	1.92	1.85

Table 2 Overall RMS error between $\mathbf{G}^{\mathrm{FHS}}(s)$ and $\mathcal{G}^{\mathrm{AVES}}\Delta(s)$

	6-DoF	11-DoF	17ord
Hover	1.45	1.57	1.66
60 knots	1.12	1.43	1.25

The third point on how effective is the input filter $\Delta(s)$ in improving the baseline simulation fidelity is the main focus of this paper. As stated in Sect. 3.1, all filters derived with this approach are unstable since they contain two right half-plane poles of the phugoid motion of $\mathbf{G}^{\mathrm{FHS}}(s)$.

Figures 15 and 16 compare the response of the baseline and updated models for 60 knots and hover, respectively. The two figures show, as an example, the response of $\mathcal{G}^{\mathrm{AVES}}\Delta(s)$ based on the 6-DoF and 17ord models. It can be observed that both 6-DoF and 17ord filters improve the simulation. Especially successful was the case of 60 knots with 17ord model where trends of all variables are almost perfectly tracked. Also, QTG limits are satisfied in this case (except small deviation towards the end in roll attitude). The 6-DoF input filter also gave very satisfying results. The match in lateral velocity is slightly better than that of 17ord, but the on-axis response in roll rate still does not have the required amplitude. Overall, the simulator model was significantly improved with both input filters.

In the hover case, improvement is also achieved but is less evident. Here the best results were obtained with the 6-DoF model, which correctly predicts the on-axis response in yaw rate. The input filter based on the 17ord model gave slightly

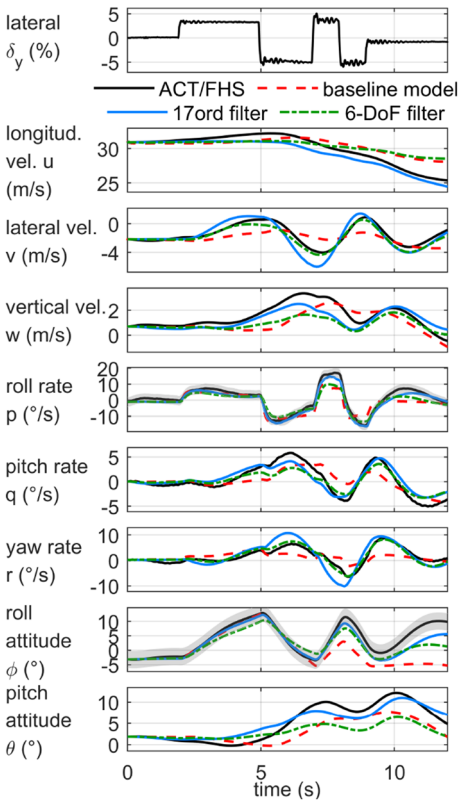

Fig. 15 Model improvements with algebraically calculated input filters at 60 knots, lateral case

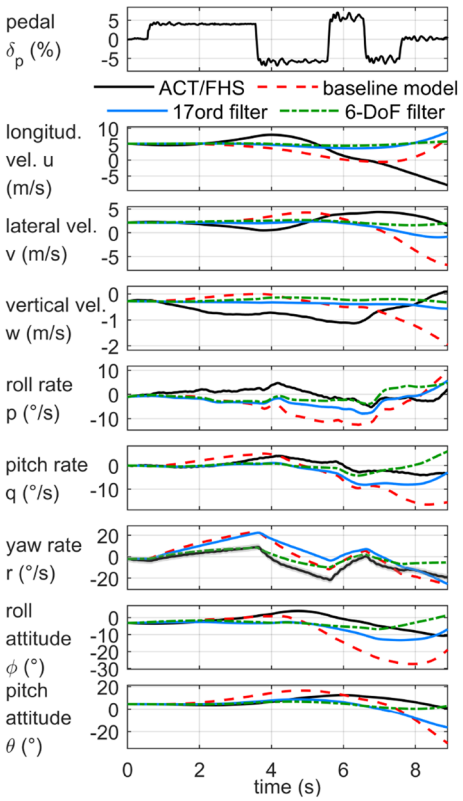

Fig. 16 Model improvements with algebraically calculated input filters in hover, pedal case

better results in pitch attitude, but it still exhibits too high amplitude in the on-axis response.

Table 3 summarizes all results for all models in terms of overall RMS error. Furthermore, the input filter was also computed by using a combination of models: 6-DoF model for canceling the AVES response and the 17ord model for the helicopter dynamics. (As a reminder from Sect. 2.6, the overall RMS for the baseline model is 4.78 for 60 knots and 7.62 for hover.)

Table 3 demonstrates that the overall simulation fidelity improved with the application of an input filter. The smallest RMS errors are achieved for the 6-DoF model in both flight conditions. Again, the RMS error value does not portray fully the reality, as confirmed in Fig. 15, where the 17ord models gave better results than 6-DoF. The mixed model

Table 3 Overall RMS error results for all updated models with algebraically calculated input filters and the baseline model

	6-DoF	11-DoF	17ord	Mixed	Baseline
Hover	6.83	7.43	7.10	7.17	7.62
60 knots	3.67	4.15	3.75	3.85	4.78

filter also gave similar results with respect to other combinations, but did not really justify its use.

For more in-depth analysis, consider Fig. 17, which exemplary shows the full results of the 6-DoF input filter against the baseline model. For 60 knots, in each axis except collective, improvements were observed. The most significant improvement was obtained in the longitudinal case. For hover, cases with lateral input were slightly degraded with the input filter. However, in all other axis, the improvements were made and especially in pedal, the inclusion of the missing dynamics was successful.

5.2 Application of controller design and filter identification

The efficiency of this approach (Sect. 3.2) depends on three points:

- the control system's performance of tracking the recorded flight test data,
- the quality of the identified transfer function model from $\mathbf{u}_{\text{ref}}$ to controller output $\tilde{\mathbf{u}}$,
- the effectiveness of the input filter $\Delta(s)$ to augment the baseline model.

To relate the controller performance to the RMS errors discussed in the previous subsection, Table 4 summarizes the overall RMS errors between the recorded outputs and the outputs of the controlled plant. These values may serve as a reference for what performance could be expected from a controller-based input filter design. Once the controller results for sweep runs are available, the frequency response from original to modified inputs is generated, forming the basis for an elementwise identification of the input filter $\Delta(j\omega) = \tilde{\mathbf{u}}(j\omega)/\mathbf{u}_{\text{ref}}(j\omega)$. An exemplary result of this fitting is shown in Fig. 18. The Bode plots of the off-axis response from δ_x to $\tilde{\delta}_y$ due to longitudinal sweeps at 60 knots and the corresponding (2, 1)-element of $\Delta(s)$ are compared. All identified input filter elements are stable, proper, and of order less or equal than five (like the one shown in Fig. 18).

Table 4 Overall RMS error between controller outputs and flight test data

	Lon	Lat	Ped	Col
Hover	1.89	1.78	1.81	1.60
60 knots	1.47	1.32	1.54	1.22

Figure 19 illustrates the time-domain effects of this input filter for a longitudinal input signal on the nonlinear simulator model at 60 knots. It can be seen that the on-axis response only slightly improved, whereas the responses in yaw rate and lateral velocity improved the most. This was in part expected since, during identification, emphasis was put on the off-axis rather than on the on-axis responses, as the controller only slightly modified the latter but noticeably modified the former. For a more in-depth analysis, Fig. 20 can be consulted, in which the RMS error is plotted for all runs. In the forward flight case, in sum, the simulation improved (the overall RMS error of the updated model is 4.4, compared to baselines 4.78), but in some cases, the performance was degraded (e.g., in the lateral axis). Best results were obtained in the longitudinal axis case. Hover condition proved to be especially arduous. Here, adding an input filter improved the simulation but not significantly. The overall RMS error for the updated model in hover amounts to 6.76, compared to baseline 7.62.

5.3 Comparison between input filters

For a deeper understanding of the filter and its modeling variants, the effects on the commanded input signals in the time and frequency domain are discussed. Figure 21 shows the time responses of the filters due to a lateral 3211 signal. These signals generated the simulator responses depicted in Fig. 15. It can be seen that the 17ord model transmits the most energy into the system, followed by the filters based on 11-DoF and 6-DoF models. It is also worth pointing out that in Fig. 21, all models exhibit a strong input in pedal (of the same order of magnitude as the lateral input), indicating

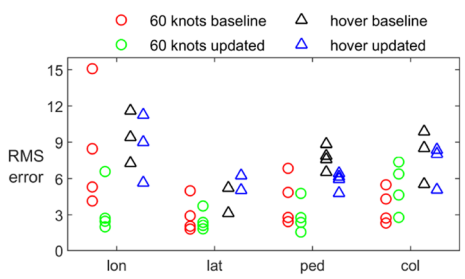

Fig. 17 RMS error comparison between the baseline and the updated model with 6-DoF input filters, for both flight conditions

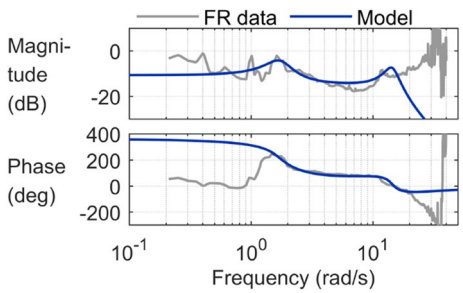

Fig. 18 Frequency responses from δ_x to $\tilde{\delta}_y$, at 60 knots

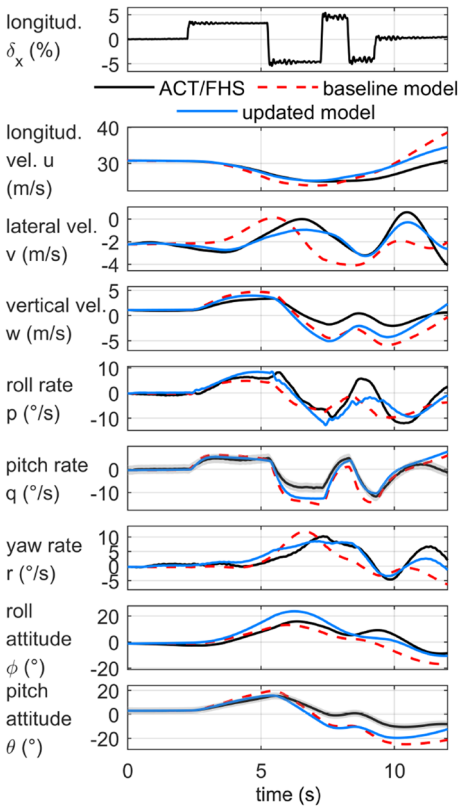

Fig. 19 Model improvements with input filter calculated based on control system results at 60 knots, longitudinal case

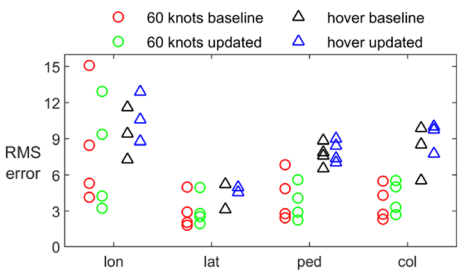

Fig. 20 RMS error comparison between the baseline and the updated model, for both flight conditions

missing coupling effects in the baseline model between lateral input and yaw response.

One way to obtain an impression of the desired frequency domain characteristics of the to-be-determined input filter is to look at the product of the inverted simulator frequency response and the helicopter frequency response. Figure 22 compares this response with those of the different input filter variants for the off-axis signal path from δ_x to $\tilde{\delta}_y$. It can be seen that the 17ord model is the closest to the theoretically calculated frequency response. Both algebraic filters show similar behavior at lower (dip in magnitude at 0.7 rad/s) but

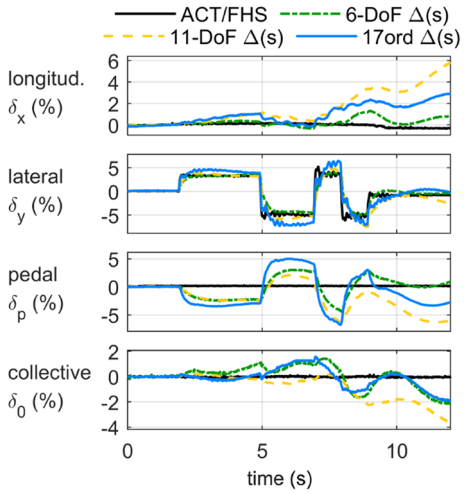

Fig. 21 Commands shaped by the input filter $\Delta(s)$

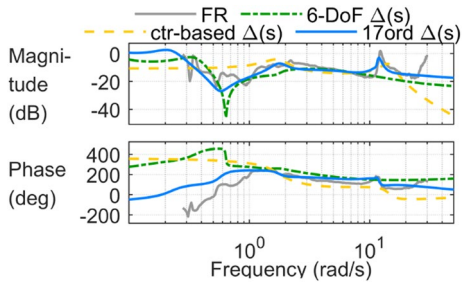

Fig. 22 Frequency response from δ_x to $\tilde{\delta}_y$, 60 knots

differ at higher frequencies. On the other hand, controller-based identified model does not capture the dip, but it contains the same resonance at 10.5 rad/s as the 17ord filter model. All models have a similar trend in the region between 1.5 and 7 rad/s.

6 Discussion

The algebraically calculated input filters can be quickly implemented once the linear models of the helicopter and simulator are available. Our results show that even when using 6-DoF models, significant improvements of the simulator fidelity can be achieved. However, higher-order effects of coupled dynamics cannot be neglected and using more degree of freedom models can be in some cases advantageous. We observed that the lower-order models gave better results when inverted than the higher-order models. Finally, high-order models usually require higher-order low-pass filters for the input filter realization leading to rather high signal energies. This altogether suggests that low-order models might be more beneficial for designing input filters.

Results showed that the filters were most successful in cases when the baseline model did not show major initial discrepancies and did not seem to lack big effects in physical modeling. An example of this is the lateral input case at 60 knots, see Fig. 15. Furthermore, the filters were also quite successful in the longitudinal input case. This indicates that the coupling effects such as pitch due to lateral control and roll due to longitudinal control are well modeled in the linear models and well captured in the matched outputs, thus they can be successfully imposed on the simulator.

An example where the input was less successful includes the case of collective input commands, for both flight conditions. This suggests that higher-order physics is not present in the baseline model, making it difficult to achieve significant improvement. Indeed, the baseline model yaw and vertical velocity responses do not include engine effects. Another issue may be that the simulation features a classical tail rotor, whereas the ACT/FHS has a Fenestron installed. This demonstrates that input filter cannot substitute important physics-modeled components of the aircraft, but rather it augments the baseline model with missing off-axis dynamics. Even when using identified helicopter models of higher order, which are specifically designed to capture engine dynamics, improvements of the baseline collective axis were modest. This leads us also to think that the outputs that we were matching may not be the most suitable to specifically improve the heave axis response. A component-wise SISO input filter can be imagined that acts on specific parts of the physics-model (for example, on the engine model) and in such way targets heave axis deficiencies.

Controller-based input filter design poses quite different challenges. Firstly, a performant control system is required. Secondly, modeling the controller input corrections is laborious and challenging. The quality of the flight test data being tracked is also crucial. If the sweep data has strongly correlated inputs (as it was the case with the ACT/FHS flight test data), which are then even more correlated through the feedback corrections, modeling such frequency data becomes difficult. A high number of flight test data sweep runs is desirable, too.

Nevertheless, using a control system to approximately invert the system might be a beneficial technique, especially in cases when no good linear models are available and, hence, an algebraic calculation of the input filter would be futile or even impossible.

For SISO systems, physical meaning can be attributed to missing dynamics with relative confidence. This is, however, difficult in the general MIMO case. Nonetheless, studying in-depth each element of missing dynamics can lead to some interesting findings. First, algebraically calculated input filters based on accurate models may match the theoretically computed 'missing' frequency response closely. Second, missing dynamics can give valuable insights into baseline model deficiencies and, hence, may motivate refined physical modeling.

7 Summary and outlook

This paper proposes a filter that corrects the pilot commands in order to reduce the mismatch between real helicopter and simulator dynamics. Two methods are presented to derive such an input filter. The first relies on good linear models for both helicopter and simulator and determines the transfer function through *direct* model inversion. The second approach is based on an explicit model-following controller, which *implicitly* inverts the simulator plant and identifies the open-loop input filter based on the closed-loop controller response. Both methods are feasible techniques to enhance model fidelity. They are easy to implement, if previous knowledge is available, and lead to measurable improvements compared to the baseline simulator performance. The filter model can be used in all applications of the simulator, from real-time pilot training flights in a certified simulator to the design of the control system in the engineering simulator.

As discussed, RMS errors can be misleading because of drift driving simulator and reference outputs slowly apart. Therefore rather trends of all important variables should be considered in order to assess the fidelity more precisely. In addition, integrated RMS cost function in frequency domain together with bounds of Maximum Unnoticeable Added Dynamics (MUAD) and evaluations based on handling quality requirements (ADS-33) can be used. However, ultimately, pilots must approve the resulting performance. This would also suggest whether unstable or stable input filters are preferred. In any case, a prerequisite for pilot tests would be an input filter for the full flight envelope. To address this, an interpolation of the missing dynamics would be necessary. The technique of model stitching [29] could be helpful in tackling this problem. Question of extrapolation of these models to other parts of the flight envelope is also open. Current solution provides an improvement at specific flying speed but in the parts of the envelope where the flight test data is not available, validity of these models should be taken with caution.

Acknowledgements The authors would like to acknowledge the work of and express their gratitude to colleague Susanne Seher-Weiß, for identifying linear models for both the helicopter and the simulator used in this study, and to thank to colleague Wolfgang von Grünhagen for his inspiration for the SISO study. The authors would also like to thank two anonymous reviewers for their helpful comments which improved the overall presentation of the paper.

Funding Open Access funding enabled and organized by Projekt DEAL.

Declarations

Conflict of interest The authors declare that they have no conflict of interest.

References

1. Tischler, M.B.: System identification methods for aircraft flight control development and validation. In: Advances in Aircraft Flight Control, pp. 35–69 (1996)
2. NATO STO: Rotorcraft flight simulation model fidelity improvement and assessment (UU) (2021). https://doi.org/10.14339/STO-TR-AVT-296-UU
3. Greiser, S.: High-fidelity rotorcraft simulation model: analyzing and improving linear operating point models. CEAS Aeronaut. J. **10**(3), 687–702 (2019)
4. Greiser, S., von Grünhagen, W.: Analysis of model uncertainties using inverse simulation. In: American Helicopter Society 69th Annual Forum. Phoenix, AZ, 21–23 May 2013
5. Thomson, D.G., Bradley, R.: The principles and practical application of helicopter inverse simulation. Simul. Pract. Theory **6**, 47–70 (1998)
6. Murray-Smith, D.J.: Inverse simulation methods and applications. In: Grand Challenges in Modeling and Simulation Conference. Edinburgh, Scotland, UK, 16–19 June 2008, pp. 143–150 (2008)
7. Rynaski, E.G.: Adaptive multivariable model following. In: Joint Automatic Control Conference. San Francisco, CA, 13–15 Aug 1980
8. Falb, P., Wolovich, W.: Decoupling in the design and synthesis of multivariable control systems. IEEE Trans. Autom. Aontrol **12**(6), 651–659 (1967)
9. Gray, G.J., von Grünhagen, W.: An investigation of open-loop and inverse simulation as nonlinear model validation tools for helicopter flight mechanics. Math. Comput. Model. Dyn. Syst. **4**(1), 32–57 (1998)
10. Seher-Weiss, S., von Grünhagen, W.: Development of EC 135 turbulence models via system identification. In: 35th European Rotorcraft Forum. Hamburg, Germany, 22–25 Sept 2009
11. Seher-Weiss, S., Tischler, M.B., Scepanovic, P., Gubbels, A.: Bell 412 system identification and model fidelity assessment for hover and forward flight. In: 8th Asian/Australian Rotorcraft Forum. Oct 2019
12. Kaletka, J., Kurscheid, H., Butter, U.: FHS, the new research helicopter: ready for service. Aerosp. Sci. Technol. **9**(5), 456–467 (2005)
13. Duda, H., Advani, S.K., Potter, M.: Design of the DLR AVES research flight simulator. In: AIAA Modeling and Simulation Technologies (MST) Conference, p. 4737 (2013)
14. Hamers, M., von Grünhagen, W.: Nonlinear Helicopter Model Validation Applied to Realtime Simulations. Forum of the American Helicopter Society (1997)
15. Wartmann, J., Wolfram, J., Gestwa, M.: Sensor fusion and flight path reconstruction of the ACT/FHS rotorcraft. CEAS Aeronaut. J. **6**, 529–539 (2015)
16. Seher-Weiss, S., von Grünhagen, W.: EC135 system identification for model following control and turbulence modeling. In: Proceedings of the 1st CEAS European Air and Space Conference. Berlin, pp. 2439–2447 (2007)
17. Wartmann, J.: Model validation and analysis using feedforward control flight test data. CEAS Aeronaut. J. **6**, 429–439 (2015)
18. Seher-Weiss, S.: ACT/FHS system identification including rotor and engine dynamics. In: American Helicopter Society 73rd Annual Forum. Fort Worth, Texas, 9–11 May 2017
19. Tischler, M.B., Remple, R.K.: Aircraft and Rotorcraft System Identification: Engineering Methods with Flight Test Examples, 2nd edn. American Institute of Aeronautics and Astronautics, Reston (2012)
20. EASA: Certification Specifications for Helicopter Flight Simulation Training—CS-FSTD(H). Initial Issue (2012)
21. Lunze, J.: Regelungstechnik 2: Mehrgrößensysteme, Digitale Regelung, 4th edn. Springer, Berlin (2006)
22. Buchholz, J.J., von Grünhagen, W.: Inversion impossible? DLR Institute report IB (2004)
23. Pavel, M.D., Jump, M., Dang-Vu, B., Masarati, P., Gennaretti, M., Ionita, A., Zaichik, L., Smaili, H., Quaranta, G., Yilmaz, D., et al.: Adverse rotorcraft pilot couplings-past, present and future challenges. Prog. Aerosp. Sci. **62**, 1–51 (2013)
24. Åström, K.J., Murray, R.M.: Feedback systems. In: An Introduction for Scientists and Engineers (2008)
25. Greiser, S., Lantzsch, R., Wolfram, J., Wartmann, J., Müllhäuser, M., Lüken, T., Döhler, H.U., Peinecke, N.: Results of the pilot "assistance system assisted low-level flight and landing on unprepared landing sites" obtained with the ACT/FHS research rotorcraft. Aerosp. Sci. Technol. **45**, 215–227 (2015)
26. Greiser, S., Lantzsch, R.: Equivalent modelling and suppression of air resonance for the ACT/FHS in flight. In: 39th European Rotorcraft Forum, Moscow, Russia, 3–6 Sept 2013
27. Schönenberg, T.: Quantitative Flugeigenschaftsbewertung des Hubschraubers EC135 FHS für ausgewählte Flugzustände nach ADS-33E. DLR Institute report IB (2010)
28. Scepanovic, P., Greiser, S.: The use of a closed loop controller scheme for the validation of nonlinear helicopter models. In: 19th ONERA-DLR Aerospace Symposium-ODAS 2019. June 2019
29. Greiser, S., Seher-Weiss, S.: A contribution to the development of a full flight envelope quasi-nonlinear helicopter simulation. In: Deutscher Luft- und Raumfahrtkongress, Berlin, 10–12 Sept 2012